Optimal flow channel structure selection for hybrid locomotive battery pack liquid cooling system

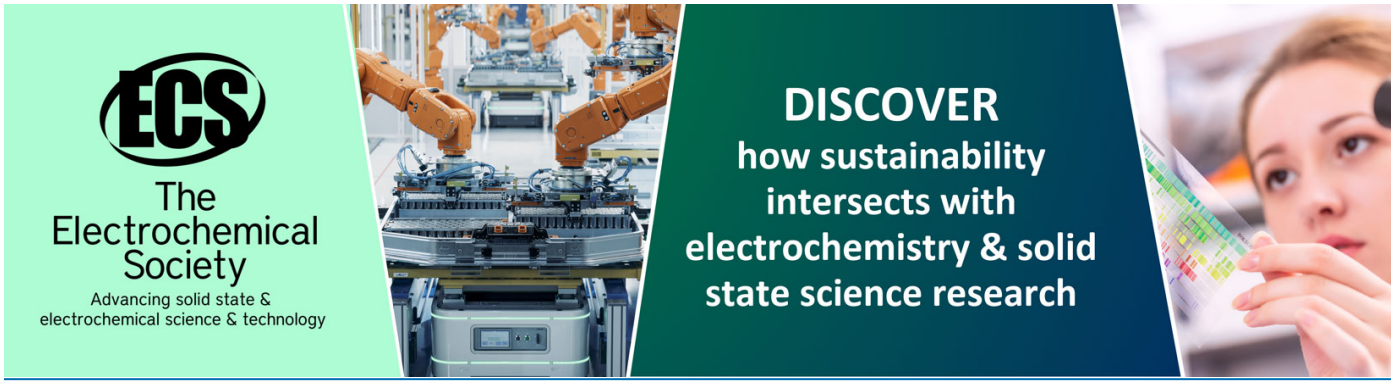

Optimal flow channel structure selection for hybrid locomotive battery pack liquid cooling system

Jichen Deng[1],Jingyang Wang[*,2],Ying Zhang[1]

1 CRRC DALIAN CO.,LTD.Dalian, China
2 School of Locomotive and Rolling Stock Engineering, Dalian Jiaotong University.Dalian, China
*Correspondence: m18356600453@163.com

Abstract. Simulation studies were performed on the power battery pack to determine the most suitable flow channel configuration for the liquid cooling system. The study involved conducting thermal simulation analysis on four different channel types with varying structures under specific conditions, including an ambient temperature of 25℃, coolant inlet speed of 2L/min, and inlet temperature of 25℃. Based on a comparative analysis, it can be inferred that an increase in the number of parallel flow channels leads to a degradation in the temperature performance of the battery pack while concurrently enhancing the pressure performance of the coolant. After considering all evaluation factors, the liquid cooling channel structure design for the battery pack was determined to consist of two parallel channels.
Keywords. Cooling system; Flow channel structure; Battery pack; Simulation analysis

1. Introduction

The power battery pack is a crucial component in hybrid locomotives,as it plays a vital role in ensuring the safe and stable operation of the vehicle.During the charging and discharging, the power battery pack undergoes repeated cycles, resulting in significant heat generation [1-3]. Given the limited space volume of the battery box, heat must be promptly dissipated to prevent adverse effects on the battery's lifespan.Failure to dissipate heat efficiently can lead to safety concerns, including fire, explosion, and other severe accidents if the temperature threshold is exceeded [4-6].Consequently, designing an effective cooling system for battery packs holds great significance.

2. Power battery pack liquid cooling system introduction

Liquid cooling is a method of cooling by utilizing a coolant to dissipate heat from a heat source. The coolant circulates through a flow channel or cold plate near the battery. The heat generated by the battery is transferred to the flow channel or cold plate through conduction, and subsequently, the coolant facilitates heat convection transfer to remove the heat. This cooling approach is characterized by relatively low manufacturing costs and enhanced security [7-8]. The present study focuses on using an indirect contact liquid cooling method. When selecting a coolant, it is advisable to choose a liquid with low viscosity and a high coefficient of thermal conductivity. Common options include water, glycol at varying concentrations, and other similar substances [9-11]. Figure 1 depicts the schematic diagram of the liquid cooling system [12].

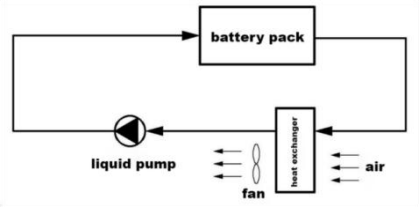

Figure 1. Schematic diagram of liquid cooling system

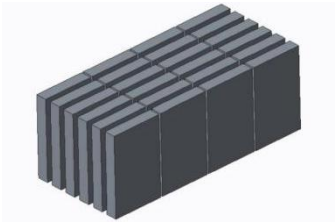

Figure 2. Battery pack layout

3. Theory of power battery heat generation and thermal parameter modeling

During the process of charging and discharging, the battery consistently generates heat. This heat can be categorized into four primary components: chemical reaction heat Q_e, Ohmic internal resistance heat Q_g, Polarized internal resistance heat Q_f, and side reaction heat Q_h [13]. The total heat of the reaction Q can be determined using the equation:

$$Q = Q_e + Q_g + Q_f + Q_h \tag{1}$$

Among the four categories above of heat, it can be observed that Among the four categories above of heat, it can be observed that the heat of side reaction Qh exhibits a relatively diminutive and inconsequential magnitude when compared to the remaining three.

The temperature distribution within the battery is influenced by both the surrounding ambient temperature and the rate of discharge[14]. Bernardi et al. [15] proposed the Battery heat generation model, which provides a more straightforward approach for calculating the heat generation rate using the following equation:

$$q = \frac{1}{V}\left[(U_0 - U) + T\frac{\partial U_0}{\partial T}\right] \tag{2}$$

Where q is the heat generation rate of the battery in W/m^3, V is the volume of the battery in m^3, U_0 and U is the open-circuit voltage and the operating voltage in V, and T is the battery's temperature in K . $\partial U_0/\partial U$is the temperature gradient, indicating temperature's effect on heat generation. In practical calculations, the value is small and negligible. U_0-U can be replaced by the product of the square of the current and the resistance [16], so the following equation can be obtained:

$$q = \frac{I^2 R}{V} \tag{3}$$

Where R is the sum of the ohmic and polarization resistance of the battery in Ω.

The parameters of the lithium iron phosphate battery are shown in Table 1.

Table 1. Battery data.

Battery Size (mm)	Rated capacity (Ah)	Densities (kg/m^3)	specific heat capacity (J/kg·K)	thermal conductivity (W/m·K)
135×35×215	50	2051.76	1232.33	λ_y=1.3 λ_x=λ_z=10.1

4. Liquid Cooling Runner Structure Program

The battery pack comprises 24 single cells organized in a 6×4 configuration, with a 5 mm separation between each cell. These gaps are filled with 18 thermal insulation boards, as depicted in Fig.2

A seven-row structure is employed for the cooling flow channels to ensure the most effective contact between single cells and the cooling flow channels. To compare the cooling effectiveness of

various flow channel structures, this study presents four schemes: serial flow channels, two parallel flow channels, four parallel flow channels, and six.

The flow channel is composed of aluminum material. The cross-sectional dimensions of the cooling flow channel are specified as 23 × 16 mm for the outer dimension and 15 × 8 mm for the inner dimension. The tube wall has a thickness of 4 mm.

The coolant was chosen as a solution of ethylene glycol with a concentration of 50%. The thermal properties of each component in the system are listed and may be found in Table 2.

Table 2. Thermophysical parameters of each part.

	makings	Densities (kg/m^3)	specific heat capacity (J/kg·K)	thermal conductivity (W/m·K)
Battery core		2051.76	1232.33	λ_x=1.3 λ_y=λ_z=10.1
flow channe	aluminum	2719	871	202
doormat	foam	320	2380	0.023
coolant	Glycol solution (50%)	1082	3300	0.4

The complete modeling of the four flow channel structures is depicted in Fig.3.

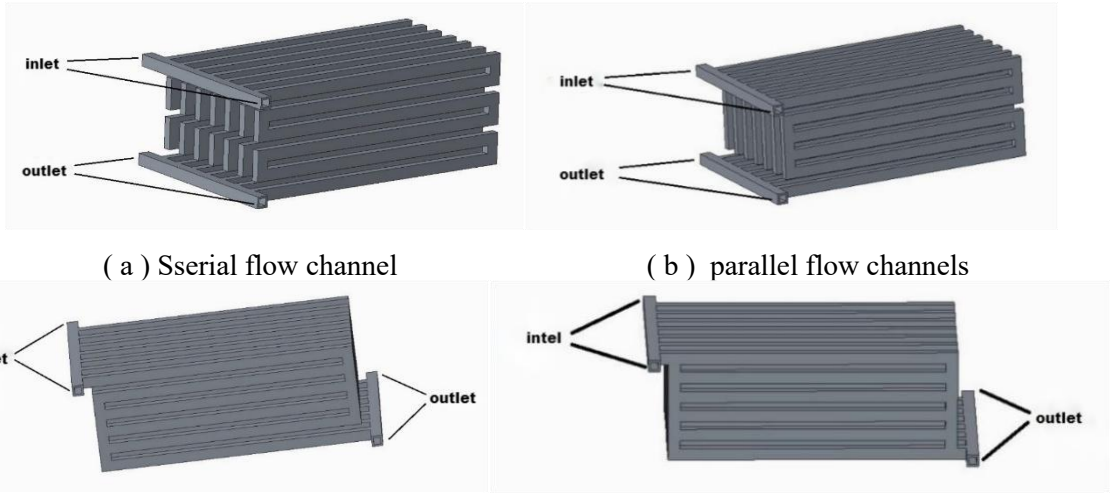

(a) Sserial flow channel (b) parallel flow channels

(c) four parallel flow channels (d)six parallel flow channels

Figure 3. Four channel models

5. Pre-treatment for thermal simulation of four types of runners

The four flow channels were imported into Ansys Fluent and subsequently meshed using an unstructured mesh (Hexa unstructured) that exhibited favorable mesh quality, as illustrated in Fig.4.

After the division of the mesh, the next step involves establishing boundary conditions.

I.Battery heat generation mode is total power, and the discharge rate is 2C; II.The ambient temperature is 25℃; III.The inlet volume flow rate is 2L/min (i.e., the inlet speed is 0.278m/s); IV.Entry temperature is 25℃; V.Air convection heat transfer coefficient is 1W / (m2·K); VI.Close the radiation, open the gravity (g = -9.81m/s2); VII.The flow state is set as turbulent (Two equation); VIII.Steady state calculation with 800 iteration steps.

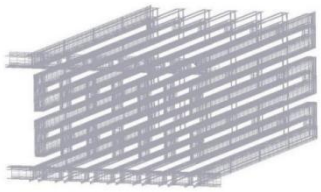

(a) Scheme one serial flow channel

(b) Scheme two parallel flow channels

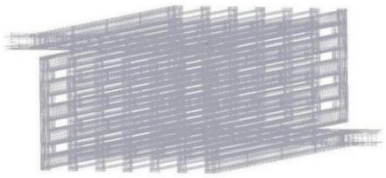

(c) Scheme three four parallel flow channels

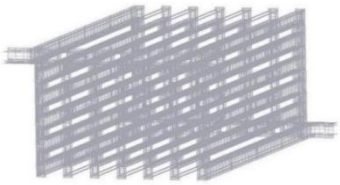

(d) Scheme four six parallel flow channels

Figure 4. Four types of channel grid division

6. Analysis of simulation results

6.1. Simulation results and setting of evaluation indicators

After the simulation calculation, the data results are shown in Table 3.

Table 3. Simulation calculation results.

	average temperature (℃)	Maximum temperature(℃)	Maximum temperature difference (℃)	dropout voltage (Pa)
Scheme1	29.14	32.52	6.92	318.45
Scheme 2	29.21	32.56	6.94	172.33
Scheme3	29.41	32.79	7.11	137.75
Scheme 4	29.52	33.71	7.94	46.87

This study sets four indicators to comprehensively assess the benefits and drawbacks of the four distinct flow channel types. These indicators encompass three temperature-related metrics: the average temperature of the battery pack, the maximum temperature, and the maximum temperature difference. A pressure indicator is also introduced, — — Coolant inlet and outlet pressure difference. These indicators effectively evaluate the cooling efficiency and power consumption performance of liquid-cooled flow.

6.2. Determination of temperature indicators

Fig.5 displays the Battery temperature field for the four different schemes. Additionally, Fig.6 illustrates the correlation between each temperature index and the number of bars in the parallel flow routes, represented as a line graph.

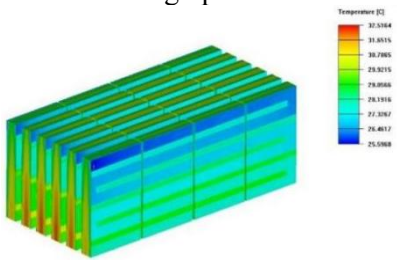

(a) Scheme one serial flow channel

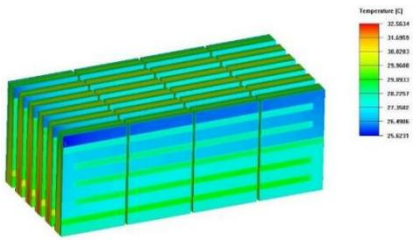

(b) Scheme two parallel flow channels

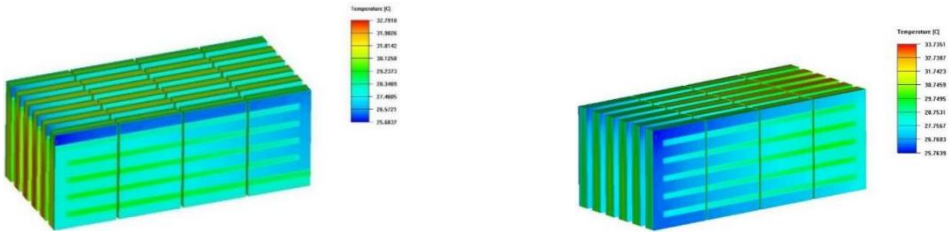

(c) Scheme three four parallel flow channels (d) Scheme four six parallel flow channels

Figure 5. Battery temperature field

It is evident from the line graph that the flow channel's cooling capability steadily declines as the number of parallel lines increases.Based on the average temperature index, Schemes 3 and 4 exhibit significantly higher values than Schemes 1 and 2. Additionally, Scheme 2 demonstrates a slightly higher average temperature than Scheme 1, although the disparity between the two is not statistically significant. Regarding the maximum temperature index and maximum temperature difference, Scheme 4 displays notably higher values than the other three programs. Conversely, Schemes 1 and 2 exhibit minimal divergence in this regard.

Using Scheme 2's two parallel flow channel structure as a standard, the results of the simulation can be used to determine that the battery pack's average temperature is only 0.2% higher than Scheme 1, 0.7% lower than Scheme 3, and 1.1% lower than Scheme 4; the battery pack's highest temperature is only 0.1% higher than Scheme 1, 0.7% lower than Scheme 3, and 3.5% lower than Scheme 4. The battery pack's maximum temperature difference is only 0.3% higher than Scheme 1. The battery pack under Scheme 2 has a maximum temperature differential of just 0.3% more than under Scheme 1, 2.4% lower than under Scheme 3, and 14.5% lower than under Scheme 4.

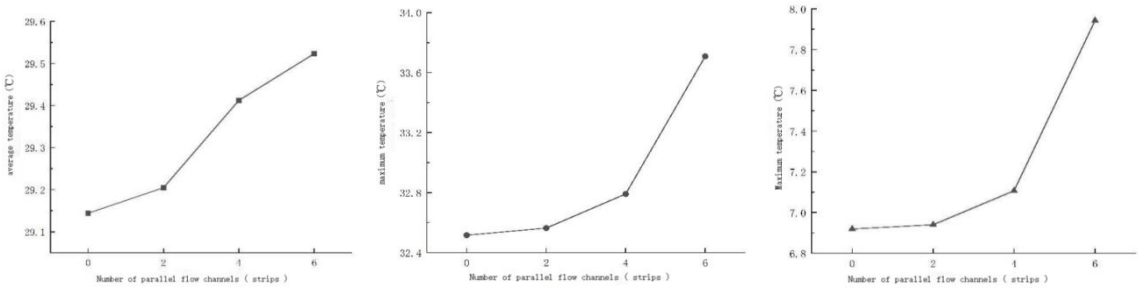

(a) Average temperature (b) Maximum temperature （c） Maximum temperature difference

Figure 6. Changes of various temperature indicators

6.3. Determination of pressure indicators

Fig.7 displays the coolant pressure fields for the four different Schemes. Additionally, Fig.8 presents a line graph illustrating the correlation between the pressure indices and the number of bars of parallel flow channels.

The graph illustrates a positive correlation between the number of parallel lines in the flow channel and the corresponding improvement in pressure performance. The disparity between inlet and outlet pressure difference in scheme 1 is significantly more significant compared to schemes 2 and 3, which, in turn, exhibit notably more considerable pressure differences than scheme 4. The discrepancy in pressure differentials between schemes 2 and 3 is relatively small.

Based on the data provided in the figure, it can be determined that the inlet and outlet pressure difference in scheme 2 is 84.8% lower compared to scheme 1, 20.0% higher compared to scheme 3, and 72.8% higher compared to scheme 4.

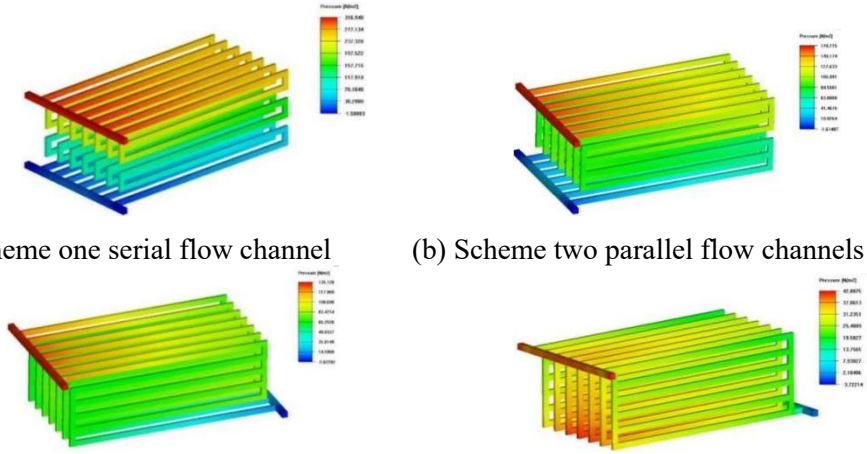

(a) Scheme one serial flow channel (b) Scheme two parallel flow channels

(c) Scheme three four parallel flow channels (d) Scheme four six parallel flow channels

Figure 7. Coolant pressure field

6.4. Determination of velocity distribution

To examine the distribution of coolant flow rate under different flow channel structure schemes, we focus on the cross-section of the middle flow channel and observe the coolant flow rate, as depicted in Fig.8.

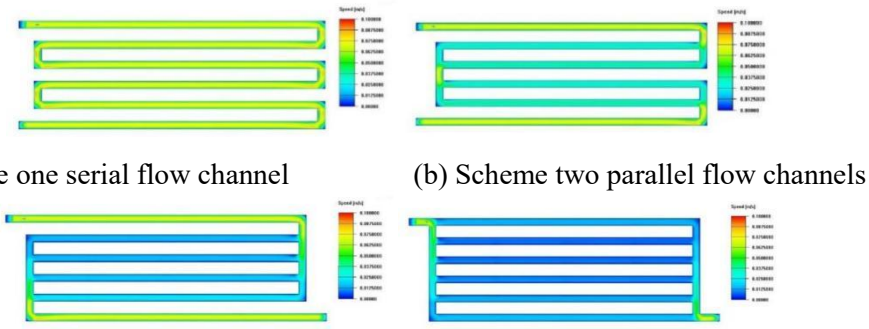

(a) Scheme one serial flow channel (b) Scheme two parallel flow channels

(c) Scheme three four parallel flow channels (d) Scheme four six parallel flow channels

Figure 8. Coolant velocity distribution

The figure illustrates that an increase in the number of parallel flow channels decreases the coolant flow rate within each channel. This effect is particularly pronounced in structures with four or six parallel flow channels, where the coolant flow rate in the middle channel is far lower than the inlet velocity. Consequently, the flow distribution within these structures is characterized by poor uniformity.

After a comprehensive examination of the parameters above, the flow channel construction plan of the liquid cooling system for the battery system has been determined to consist of two parallel flow channels, as depicted in scheme 2.

7. Discussion

The conclusions of this study indicate that the number of parallel channel lines somewhat impacts the battery pack's temperature performance and the coolant's pressure performance.

The following conclusions are reached using the simulation calculation and analysis of the temperature field and coolant pressure difference of the battery pack under the four channel schemes: as the number of parallel channels increases, the performance of the liquid-cooling channels in terms of cooling declines gradually, the power consumption performance improves slowly, and the coolant velocity distribution in the channels drops gradually.

The research examines two parallel flow channel topologies. The pressure performance of these channels is substantially better than the serial flow channel's, and the temperature performance is not that much different. It matters a little while choosing the liquid cooling system's flow channel for the hybrid locomotive's battery pack. However, the parallel runner structure examined in this study might not be relevant in all circumstances since it does not simulate and evaluate the battery pack's temperature field and the coolant's pressure differential under different environments.

8. conclusion

After simulation computation and analysis of the temperature field and coolant pressure differential of the battery pack under four flow channel schemes, the following results are drawn in this paper:

(1) As the number of parallel flow channels in the battery pack increases, there is a corresponding increase in the average temperature, maximum temperature, and maximum temperature difference. This suggests a gradual deterioration in the cooling efficiency of the liquid-cooled flow channels. Furthermore, when the number of parallel flow channels reaches six, there is a notable and significant increase in the battery pack's maximum temperature and maximum temperature difference；

(2) As the number of parallel flow channels increases, there is a noticeable decrease in the Coolant inlet and outlet pressure difference. This suggests an improvement in the power consumption performance of the liquid-cooled flow channels. Furthermore, there is a significant and distinct difference in the pressure difference values among the four schemes being compared；

(3) As the number of parallel flow channels increases, the velocity distribution of the coolant in the flow channel deteriorates, and the structure with numerous parallel flow channels has an uneven velocity distribution；

(4) The most suitable liquid-cooling flow channel structure scheme for this battery pack is using two parallel flow channels. This configuration exhibits superior temperature performance compared to four parallel runners and six parallel flow channels. Additionally, the temperature performance of the two parallel flow channels is comparable to that of serial flow channels. Furthermore, the pressure performance of the two parallel flow channels is superior to that of serial flow channels；

In future work, the temperature field of the battery pack and the difference in coolant pressure in different environments can be simulated and analyzed while considering whether the cooling rate is too fast or too slow for transient simulation calculations.

9. References

[1] Heli Wang , Yunsheng Xie,Chenglong Luo.Greenhouse gas emission status and reduction measures of transportation industry [J]. Energy Research and Management, 2011(003):000.

[2] Rui Tian,Yinan Kang. Development of hybrid electric locomotives at home and abroad (Part II)[J]. Foreign Railway Locomotive and Motor Car, 2012.

[3] TianZheng Tian,Huimin Peng. Japanese HD300-901 hybrid electric locomotive sample [J]. Foreign Railway Locomotive and Motor Car, 2011.

[4] Changfu Peng,Shunguo Liu,Cong Ren.Design and test of CKD6E5000 hybrid electric locomotive [J]. Railway Locomotive and Motor Car, 2012 (10):5+27-29.

[5] YufaMeng , GuofuHe ,Shunguo Liu.Study on adaptability, economy and environmental protection of shunting operation of HXN6 hybrid shunting locomotive [J]. Railway Locomotive & Car, 2018, 38(1):6.

[6] Pesaran A A . Battery thermal management in EVs and HEVs: Issues and Solutions. 2001.

[7] LipingLiu, Jianqiang Bao. Cooling methods for concentrating solar cells [C]//. Proceedings of the 2009 Annual Conference of Shanghai Institute of Refrigeration.2009:151-153.
[8] YingPeng, Rui Huang,Xiaoli Yu, JianqingXu. Comparative study on cooling schemes of lithium-ion power batteries for electric vehicles [J]. Journal of Mechanical & Electrical Engineering,2015, 32(04):537-543.
[9] Anthony Jarrett,Il Yong Kim. Design optimization of electric vehicle battery cooling plates for thermal performance[J]. Journal of Power Sources,2011,196(23).
[10] Shiyu Wang, Fengxiang Ling , Jianfeng Sun, Yimin Yan, LongLi . Paraffin composite phase change materials and the research progress of thermal properties [J].Contemporary Chemical Industry, 2015, 44 (7) : 1598-1601. The DOI: 10.13840 / j.carol carroll nki cn21-1457 / tq. 2015.07.045.
[11] Shangan Zhang . Research on liquid cooling and heat dissipation mechanism of lithium battery pack for hybrid electric vehicle [D]. Hunan University,2013.
[12] Yeow K , Teng H , Thelliez M , et al. Comparative study on thermal behavior of lithium-Ion battery systems with indirect air cooling and indirect liquid cooling[C]// Asme/iscie International Symposium on Flexible Automation. 2012:585.